Perturbing Hele-Shaw flow with a small gap gradient

H. Zhao, J. Casademunt, C. Yeung, and J. V. Maher
Department of Physics and Astronomy, University of Pittsburgh, Pittsburgh, Pennsylvania 15260
(Received 5 August 1991)

A controlled perturbation is introduced into the Saffman-Taylor flow problem by adding a gradient to the gap of a Hele-Shaw cell. The stability of the single-finger steady state was found to be strongly affected by such a perturbation. Compared with patterns in a standard Hele-Shaw cell, the single Saffman-Taylor finger was stabilized or destabilized according to the sign of the gap gradient. While a linear stability analysis shows that this perturbation should have a negligible effect on the early-stage pattern formation, the experimental data indicate that the characteristic length for the initial breakup of a flat interface has been changed by the perturbation.

PACS number(s): 47.20.−k, 68.10.−m

I. INTRODUCTION

The Saffman-Taylor (ST) problem [1] has been studied intensively [2] since Saffman and Taylor published their classic paper in 1958. The problem consists of studying the interfacial patterns between two fluids which are driven either by applied pressure or by gravity in a narrow gap between two parallel glass plates (a Hele-Shaw cell [3]). For Newtonian fluids, the flow can simply be modeled by Darcy's law, i.e., the velocity of the fluid is proportional to the pressure gradient. For this reason, the ST problem has a very close relation with studies of viscous fingering in porous media. The pressure obeys the Laplace equation and the boundary conditions can be written down easily. The dynamical equations are usually called the Hele-Shaw equations for this ST problem [4–6].

In the problem of directional solidification (DS) [7], the situation is different. The bulk equation is a diffusion equation in a moving reference frame. Even within the quasisteady approximation, this is different from the bulk equation of ST flow. In addition, the boundary conditions introduce an extra length scale in DS, so the pattern morphology in DS is richer than in ST flow.

Ben-Jacob *et al.* [8] have pointed out that the ST problem can be brought closer to DS by adding a linear gradient term in the gap of the Hele-Shaw cell. Couder and co-workers [9–11] have extended this reasoning to study flow between two paraxial rotating cylinders as an analogue of DS. They have been able to study cellular structures which are reminiscent of those seen in DS, but their morphology diagram also includes other effects which are not normally seen in DS and which seem to arise from the fluid mechanical nature of their boundary conditions.

When a gradient term is added to the gap of the Hele-Shaw cell, a controllable perturbation is introduced into the ST problem. The dynamical equation and boundary conditions can be easily written down in the same manner as in the ordinary Saffman-Taylor problem and are somewhat simpler than in the paraxial cylinder case of Couder and co-workers (with the attendant disadvantage that the average position of the interface must travel through the cell). However, since a new length scale is introduced by the perturbation term, the system should be richer than the ST problem. Although the resulting equations are formally similar to DS, the analogy with solidification only holds for a restricted range of parameters. Accordingly, nonparallel ST flow may introduce new richness through the effective time and space dependence of the analogues of the parameters of DS. At the same time, as this is a fluid system, we have much better control of the experimental conditions than in DS.

In this paper, we report our studies of effects of a linearly varying gap perturbation on the ST flow problem. We see how the stability of the single-finger configuration and the initial breakup of the flat interface have been changed by the presence of this perturbation.

II. THE MODEL EQUATIONS

The dynamical equations for flows in a Hele-Shaw cell with a gap gradient are as follows: Let the Hele-Shaw cell lie in the x-z plane, and the flow be in the positive z direction. The gap at position z is $b(z)=\bar{b}+b'z$, where b' is the gradient of the gap which can be either positive or negative. The Darcy equation is obtained in a similar manner as for the parallel-plate case [11]:

$$\mathbf{v}=-\frac{[b(z)]^2}{12\mu}\nabla_h P\,, \tag{1}$$

where $\mathbf{v}$ is the velocity of flow averaged across the gap, P is the pressure in the fluid, μ is the fluid's shear viscosity, and ∇_h is the two-dimensional gradient in the x-z plane. Incompressibility of the invaded fluid ($\nabla_h\cdot b\mathbf{v}=0$) results in a differential equation for P,

$$\nabla_h^2 P+\frac{1}{\ell_D(z)}\frac{\partial P}{\partial z}=0\,, \tag{2}$$

with $\ell_D(z)=b(z)/3b'$. The pressure drop at the interface is

$$P_i=\sigma\kappa-\sigma\frac{c}{b(z)}\,, \tag{3}$$

where κ is the curvature in the x-z plane, σ is the surface tension, and c is a wetting parameter which relates the sign and gap dependence of curvature in the gap di-

rection. Here we have ignored all kinetic terms in the boundary condition. The normal velocity of the interface is given by

$$\hat{\mathbf{n}} \cdot \mathbf{v}_i = -\frac{[b(z)]^2}{12\mu} \frac{\partial P}{\partial n} , \tag{4}$$

where $\hat{\mathbf{n}}$ is the normal to the interface directed into the invaded fluid. These equations are without approximations other than the standard ones used to obtain the Hele-Shaw equations.

As shown by Ben-Jacob *et al.* [8], the perturbed Hele-Shaw equations with a gap gradient can be brought closer to the DS equations when b' is small. We introduce a dimensionless pressure $p = P b_0/12V_0\mu$. Here V_0 is the mean rate of advance of the interface and is defined as

$$V_0 = \frac{1}{a} \int ds\, \hat{\mathbf{n}} \cdot \mathbf{v}_i , \tag{5}$$

with a being the width of the cell. $z_0(t) = V_0 t$ is the average position of the interface at time t and $b_0 = b(z_0)$. Let $\xi(x,t) = z_i(x,t) - z_0(t)$ be the deviation of the interface $z_i(x,t)$, at x and time t, from the average interface position $z_0(t)$. Expanding in the parameter $b'\xi/b$ we get

$$\nabla_h^2 p + \frac{1}{\ell_D} \frac{\partial p}{\partial z} = 0 , \tag{6}$$

where, to lowest order, $\ell_D = b(z_0)/3b'$ can be considered independent of ξ. The lowest-order contribution to the pressure drop is

$$p_i = d_0\kappa - \frac{1}{\ell_T}\xi , \tag{7}$$

where a capillary length d_0 is defined as

$$d_0 = \frac{\sigma b_0}{12V_0\mu} \tag{8}$$

and

$$\ell_T = -\frac{12\mu b_0 V_0}{c\sigma} , \tag{9}$$

ℓ_D and ℓ_T are the analogs of the diffusion length and thermal length in the DS. To lowest order the continuity condition is

$$\hat{\mathbf{n}} \cdot \hat{\mathbf{z}} \left(1 + \frac{1}{V_0}\frac{\partial \xi}{\partial t}\right) = -\left(1 + \frac{2}{3}\frac{\xi}{\ell_D}\right) \frac{\partial p}{\partial n} . \tag{10}$$

We see that the current problem has three length scales: a diffusion length, a thermal length, and a capillary length. With the exception of an extra term in the right-hand side of Eq. (10), these length scales come into the equations in the same manner as in DS [7]. The lengths can be independently tuned by changing liquids and cell geometry, which allows us to access values of parameters inaccessible to DS. For example, since the diffusion length is not directly related to the average velocity V_0, the interface can be unstable for arbitrary signs of the ℓ_D and ℓ_T. Another important difference is that the average position of the interface changes with time. Therefore the parameters ℓ_D, ℓ_T, and d_0 are effectively time dependent. This implies that there is no true steady state. Furthermore, higher-order corrections to Eqs. (6)–(10) would introduce spatial dependence in those parameters.

In this experiment, we study a nonwetting fluid invading a wetting fluid, making c positive and giving ℓ_D and ℓ_T the opposite sign. This situation is therefore inherently different from the ordinary DS.

III. THE EXPERIMENT

The experiment was performed using a rectangular Hele-Shaw cell of width 39 cm and length 120 cm. We varied the Teflon spacers in the cell to achieve five gradients: -3.0×10^{-3}, -1.5×10^{-3}, 0 (which is a parallel plate cell), 1.5×10^{-3}, and 3.0×10^{-3}. We could change the initial gap in the range $1.5 \leq b \leq 4.6$ mm by initiating the flat interface at different positions along the length of the cell.

All flows reported in this paper involved nitrogen gas invading heavy paraffin oil in the Hele-Shaw cell. As was noted above, the heavy paraffin oil completely wets the glass plates of the cell in the presence of nitrogen gas so $c = 1$. All flows were operated very close to constant volumetric injection rate. The shear viscosity of heavy paraffin oil is 65 cP (manufacturer given value [12]) and the interfacial tension between the oil and nitrogen is measured by the capillary rise method to be 29.5 dyn/cm at room temperature. To give an indication of typical parameter values, if $b_0 = 0.22$ cm and $b' = 3.0 \times 10^{-3}$, then $d_0 = 1$ cm, $\ell_D = 24$ cm, and $\ell_T = -20$ cm for $V_0 = 1$ cm/sec. The patterns of late-stage single fingers were captured by a 35-mm single-lens reflex camera, and the early stage patterns were recorded by a charge-coupled device television camera and stored on videotape.

IV. RESULTS AND DISCUSSION

A. Steady state

Strictly speaking there is no true steady state in this experiment. However, we find that the single-finger configurations roughly maintain their shapes for a significant period of time. The tip-splitting instability that we study occurs before we see any significant change in the shape of these quasisteady fingers. Therefore we will treat these as steady states.

The morphology is affected by the perturbation b' but the most drastic effect is in the stability of the single finger. When $b' < 0$, the steady-state finger turns into one with a sharper tip (see Fig. 1) which stays stable up to much larger advancing speed than is required to destabilize the finger if $b' = 0$. When $b' > 0$, the steady-state finger is converted to one which exhibits a flattened tip [see Fig. 2(a)] and tip splitting occurs easily at advancing speeds much lower than those needed to destabilize the $b' = 0$ case [see Fig. 2(b)].

In order to measure how unstable the tip has become, we define a length D which is the distance between successive tip-splitting events. This is approximately constant for whatever number of tip splittings can be ob-

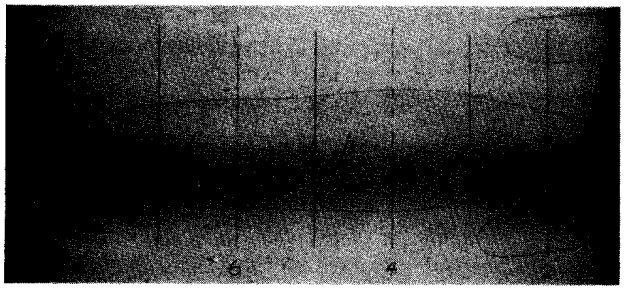

FIG. 1. Pattern formed in a Hele-Shaw cell with gap gradient $b' = -1.5 \times 10^{-3}$. If $b' = 0$, the finger would be stable at this driving velocity but would also be fatter at the tip and more uniform along its length.

served in the length of the Hele-Shaw cell. Figure 3 shows the results of D versus V_0 for the five different gradients. The lines are best-fit curves through data of each gradient. Only data for $b' = 0$ are shown on the graph, but the scatter of data points for other gradients is similar to the $b' = 0$ case. From Fig. 3, we can easily see how the small perturbation b' has affected the stability of the single-finger steady state. The value of D represents the spatial frequency of occurrence of tip splitting, thus its inverse is a rough measure of the strength of instability of the ST steady-state finger. Figure 3 shows that D decreases as V_0 increases for all five different gap gradients, which is simply the effect of changes of the capillary number due to the increase of V_0. Compared with the constant gap case, $b' > 0$ reduces D, and thus increases the frequency of tip splitting; $b' < 0$ increases D, and thus reduces the

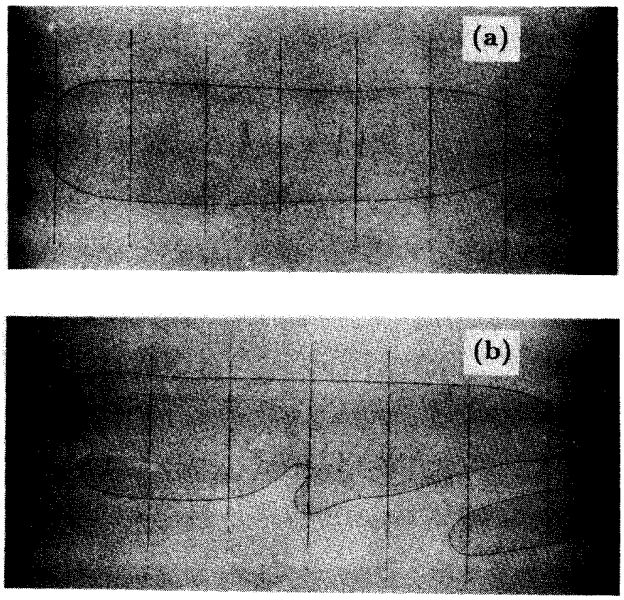

FIG. 2. Patterns formed in a Hele-Shaw cell with gap gradient $b' = 1.5 \times 10^{-3}$. (a) At low driving velocity, no tip-splitting occurs, but the finger exhibits a flattened tip. (b) Tip-splitting occurs at a driving velocity at which the finger would be stable if $b' = 0$.

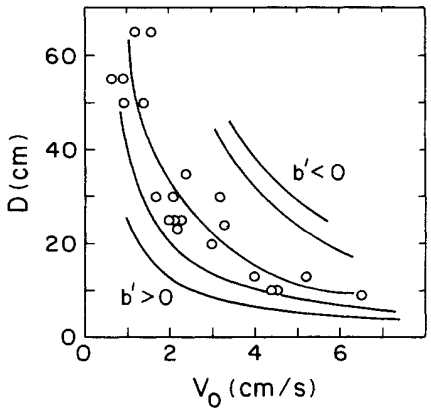

FIG. 3. Best fit curves through data of D vs V_0 for five different gradients: $b' = -3.0 \times 10^{-3}$, -1.5×10^{-3}, 0, 1.5×10^{-3}, 3.0×10^{-3} (from upper right to lower left). Only data for $b' = 0$ are shown in the graph. The scatter of other data is similar.

frequency of tip splitting. For the parallel ST flows, the strength of instability of the steady-state finger can also be indicated by a threshold of advancing speed below which tip splitting does not occur. In our experiment the threshold is not necessarily constant due to the net advance of the interface. However, we can estimate an effective threshold by observing the advancing speed below which the steady-state finger travels through the whole length of our cell without destabilizing. This threshold velocity is shown as V_T versus b' in Fig. 4. Our observation indicates that b' has notably affected this necessary velocity with $b' > 0$ ($b' < 0$) decreasing (increasing) the threshold. The relation between the threshold and the b' is not a simple linear one. In fact we observe that the threshold velocity seems to change abruptly near $b' = 0$.

Having introduced the empirical results, we now attempt to provide at least qualitative discussion of their important features. We first discuss the morphology of the steady state. It is well known that the steady state is very sensitive to small perturbations such as placing a bubble at the tip [13]. Therefore it may not be surprising that we observe a change in the shape. The trends

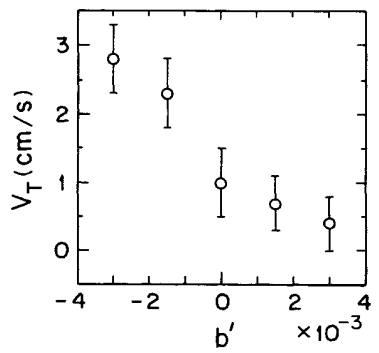

FIG. 4. The threshold velocity V_T of finger instability vs the gap gradient b'.

observed can be roughly explained by noticing the fact that, for $b' < 0$, incompressibility implies that the velocity of the fluid in the tip region will be larger than the velocity behind it. This net acceleration of the tip will stretch the tip in the flow direction relative to the ST finger, thereby producing a sharper finger. On the other hand, for $b' > 0$, the opposite will occur and the finger will be flattened.

Now we consider the stability of fingers. It is interesting to note that the results cannot be explained by an adiabatic argument based on an instantaneous capillary number Ca= $(a/b)^2(V_0\mu/\sigma)$. For $b' > 0$ the effective Ca seen by the tip decreases as the tip advances. In addition since we apply an approximately constant injection rate during our flow realizations, V_0 decreases during our flow realization, further reducing the capillary number. For $b' < 0$ the effective Ca would increase. Therefore such an argument would predict that the finger will become more stable (unstable) with time for $b' > 0$ ($b' < 0$). While we do not know what effects would be produced on the stability of the finger if a kinetic term were added to Eq. (3), we note that the first expected effect would be a reduction in the magnitudes of tip acceleration relative to the case without the kinetic term (e.g., faster tips would produce larger pressure jumps). Thus the simplest effect of including a kinetic term might be to bring the finger back closer to the parallel-plate case and thus would not, at least at first glance, be expected to furnish an explanation of our results.

To understand the stability of the finger we recall the mechanism by which the parallel-plate Saffman-Taylor fingers are stabilized [4]. In that case, the disturbances at the tip propagate backwards along the side of the finger where they are dampened away. The experimental results could be explained by a modification of the efficiency of this process associated with the fact that the tip is being accelerated relative to the region behind it. Accordingly, a perturbation will be removed from the tip faster if $b' < 0$ and slower if $b' > 0$. Furthermore, the changes in the morphology also contribute in the same direction to the stability of the finger. If the tip is flatter the disturbances have more time to grow before leaving the tip region. This implies that the finger would be less stable which is consistent with the experiments. If the tip is sharper the disturbances can be easily swept away from the tip region resulting in a more stable tip.

B. Linear regime

We have performed a linear stability analysis for a flat interface in this system and obtained the following dispersion relation:

$$\omega(k) = \frac{V_0}{2|l_D|}\left[\left(1 - \frac{b_0}{l_T} - d_0 b_0 k^2\right) \times [S(l_D) + \sqrt{1 + 4l_D^2 k^2}] - \tfrac{2}{3}S(l_D)\right], \tag{11}$$

where $S(\ell_D)$ is the sign of ℓ_D. Putting numerical values for the parameters accessible to our experiment, we find that this dispersion relation predicts no observable dependence on b'. That is, Eq. (11) predicts essentially the same numerical values of $\omega(k)$ as the parallel ST flow,

$$\omega(k) = V_0\left(1 - \frac{b^2\sigma}{12\mu V_0}k^2\right)|k|\,. \tag{12}$$

To test the behavior of the system in the initial stages of breakup of a flat interface we have defined our average wavelength λ by dividing the width of the Hele-Shaw cell by the number of fingers that are present at the earliest stage of pattern development. For each flow realization, in addition to λ we know V_0, the speed of advance of the initial flat interface, b' and b_0, the gap in the cell at the point where flow is initiated. Unexpectedly, after measuring many flow realizations covering many values for V_0, b', and b_0, we find a significant dependence of the initial breakup of a flat interface on the magnitude of b' but not its sign.

Figure 5 shows that we observe no dependence of λ on the sign of b'. The open circles are values of λ measured with $b' = 3.0 \times 10^{-3}$ while the solid triangles come from flows with $b' = -3.0 \times 10^{-3}$. The solid line is the maximum growth rate wavelength from the dispersion relation [Eq. (11) or (12)], and the dashed line is the cutoff wavelength from the dispersion relation. The experimental values of λ show a different slope than predicted by the dispersion relation, migrating from near the expected fastest growing mode to slightly below the expected cutoff as velocity is reduced. All our attempts to explain this in terms of experimental imperfection have failed; particularly convincing is the fact that most possible sources of experimental error such as our growing uncertainty of the position at which the planar interface becomes unstable

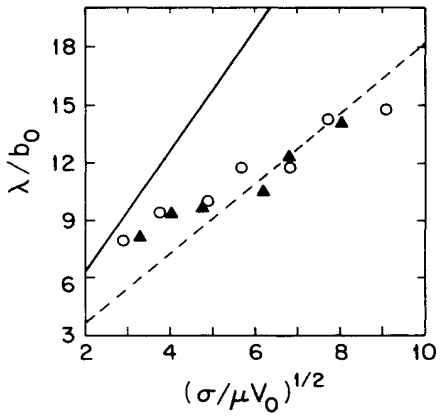

FIG. 5. λ/b_0 vs $(\sigma/\mu V_0)^{1/2}$ for the cases $b_0 = 3.4$ mm, and two gap gradients of the same magnitude but different signs, $b' = \pm 3 \times 10^{-3}$. The solid (dashed) lines are from the modes of maximum (cutoff) growth rates of the numerical solutions of the dispersion relation. The open (solid) points are experimental data of positive (negative) b'. The data support the dispersion relation in predicting the independence of the wavelength from the sign of the gap gradient. All of our flow realizations show this feature.

as V_0 is reduced (since the interface travels farther before becoming observably unstable) would push the data in different directions for different signs of b'. The robustness of all our results against changes in the sign of b' adds strength to all the parameter dependence of λ discussed below.

Figure 6 shows a typical dependence of λ on the magnitude of b'. The data are for $b_0 = 3.4$ mm (except for those of $b' = 0$ where $b_0 = 3.0$ mm). When $b' = 0$ the typical λ observed is slightly greater than the value for the fastest growing wavelength. (The dispersion relations were evaluated using values of viscosity given by the manufacturer and surface tension measured for our oil by the capillary rise method. The uncertainty in σ is sufficiently large that we could easily adjust the dispersion relation maximum to lie on the $b' = 0$ experimental values of λ, pushing even more of the $b' \neq 0$ data beyond the cutoff wavelength, but we have instead used our measured value of σ for all calculations.) The solid triangles come from $b' = -1.5 \times 10^{-3}$ flows; these have a smaller slope than for $b' = 0$ and always lie below the expected fastest growing wavelength. This trend is accentuated for $b' = -3.0 \times 10^{-3}$ (open circles) where the observed λ is generally near the expected cutoff wavelength.

Figure 7 shows the dependence of λ on b_0. The solid lines are expected fastest growing wavelengths as b_0 changes. The data change more drastically in both relative spacing and slope than would be expected from the dispersion relation, as is shown for $b' = 3.0 \times 10^{-3}$. As was mentioned above, this effect, like all the others we have discussed for Figs. 5–7, appears for both signs of b' and so cannot easily be ascribed to uncertainty in the proper choice of b_0.

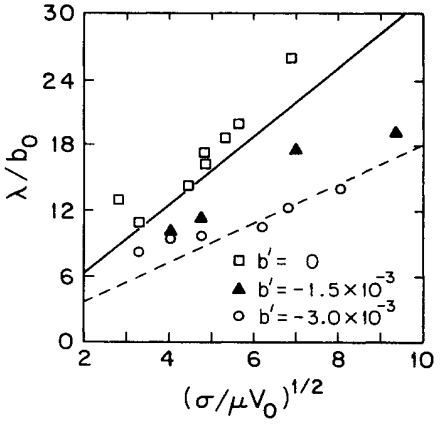

FIG. 6. λ/b_0 vs $(\sigma/\mu V_0)^{1/2}$ for the cases $b_0 = 3.4$ mm, and two gap gradients of the same signs but different magnitudes. The solid (dashed) lines are from the modes of maximum (cutoff) growth rates of the numerical solutions of the dispersion relation. The open (solid) points are experimental data for $b' = -1.5 \times 10^{-3}$ ($b' = -3.0 \times 10^{-3}$). The dispersion relation makes no distinction between the two different gap gradients, but the experimental data clearly show that there is some difference between the two. The data with $b' = 0$ and $b_0 = 3.0$ mm are also plotted for comparison in this figure as square points.

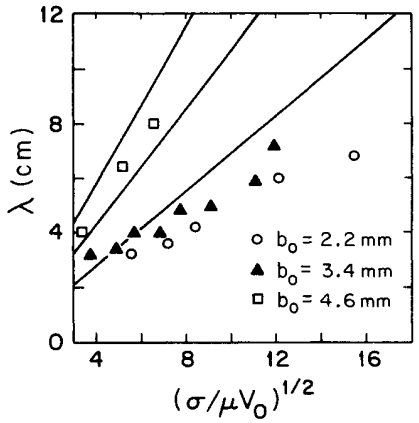

FIG. 7. λ vs $(\sigma/\mu V_0)^{1/2}$ for the cases $b' = 3 \times 10^{-3}$ and three different initial gaps. The circle, solid triangle, and square points are experimental data of b_0 =2.2, 3.4, and 4.6 mm, respectively. The solid lines are from the modes of maximum growth rates of the numerical solutions of the dispersion relation.

All our results are summarized in Fig. 8. This figure is less easy to read than the others, since λ measurements for many values of b_0 and V_0 are superposed for all five values of b'. However, using the scaling suggested by the dispersion relation allows us to show that all the data taken together support the general features illustrated in Figs. 5–7. That is, when we plot λ/b_0 versus $(\sigma/\mu V_0)^{1/2}$ we expect the fastest growing wavelength to follow the solid line and we expect a cutoff wavelength at the dotted line. The data for $b' = 0$ (triangles) run parallel to and slightly above the solid line. The data for $b' = \pm 1.5 \times 10^{-3}$ (circles) have slightly lower slope and

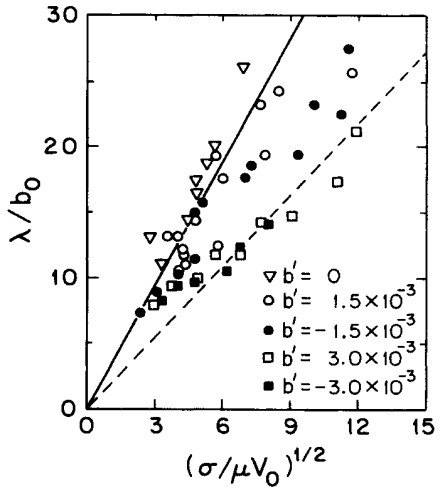

FIG. 8. Scaled data of λ/b_0 of many different initial gaps vs $(\sigma/\mu V_0)^{1/2}$ for five different gap gradients. The solid (dashed) lines are from the modes of maximum (cutoff) growth rates of the numerical solutions of the dispersion relation. The points are experimental data with the values of b' indicated in the legend.

lower absolute values in the range of observation, and the data for $b' = \pm 3.0 \times 10^{-3}$ (squares) lie lowest and with lowest slope of all, frequently lying below the predicted cutoff wavelength.

We have no simple explanation for the origin of the effects illustrated in Figs. 5–8. The nonparallel-plate case is clearly different from the parallel case in that the wavelength selected is significantly different from the most unstable mode predicted by the linear analysis. This suggests that early nonlinear effects can play an important role in the selection of the observed wavelength. While the inclusion of kinetic terms in this analysis may be important for understanding the results, it should be noted that the dispersion relation without kinetic effects gives very accurate results for the parallel-plate case even though kinetic effects are known to affect the steady-state solution in the parallel-plate case.

V. CONCLUSIONS

We have observed the single-finger configurations to be strongly affected by adding a small gradient b' in the gap of the Hele-Shaw cell. For positive b' the tip is flatter and more unstable relative to the $b' = 0$ case. For negative b' the tip is sharper and more stable. Adiabatic arguments predict the wrong trend for the stability suggesting that the mechanism by which the perturbations are removed from the tip region is very sensitive to this perturbation in the gap.

The linear analysis predicts that b' produces no observable effect for the parameters used in this experiment. However, an important difference from the $b' = 0$ case was observed in that the characteristic length in the early stages of the instability is significantly different from the most unstable mode. This difference depends only on the magnitude of b' but not on the sign and changes at a systematically different rate as V_0 is varied.

ACKNOWLEDGMENTS

We acknowledge helpful discussions with D. Jasnow, P. D. Gallagher, T. Rogers, and J. Viñals. H.Z. thanks K. V. McCloud for assistance during final stage of the experiment. This work was partially supported by the U.S. Department of Energy under Grant No. DE-FG02-84ER45131 (H.Z. and J.V.M.). J.C. acknowledges the Ministerio de Educación y Ciencia (Spain) for a Fulbright grant and support from NATO Collaborative Research Grant No. 900328. C.Y. is grateful to the National Science Foundation through the Division of Materials Research for support under Grant No. DMR89-14621.

[1] P. G. Saffman and G. I. Taylor, Proc. R. Soc. London Ser. A **245**, 312 (1958).

[2] R. L. Chuoke, P. van Meurs, and C. van der Poel, J. Petrol. Tech. **11**, 64 (1959); J. W. McLean and P. G. Saffman, J. Fluid Mech. **102**, 455 (1981); D. A. Kessler, J. Koplik, and H. Levine, Phys. Rev. A **30**, 3161 (1984); D. A. Kessler and H. Levine, *ibid.* **32**, 1930 (1985); D. Bensimon, *ibid.* **33**, 1302 (1986); S. Sarkar and D. Jasnow, *ibid.* **35**, 4900 (1987); A. T. Dorsey and O. Martin, *ibid.* **35**, 3989 (1987); B. I. Shraiman, Phys. Rev. Lett. **56**, 2028 (1986); D. C. Hong and J. S. Langer, *ibid.* **56**, 2032 (1986); J. V. Maher, *ibid.* **54**, 1498 (1985); S. A. Curtis and J. V. Maher, *ibid.* **63**, 2729 (1989).

[3] H. J. S. Hele-Shaw, Nature (London) **58**, 34 (1898).

[4] D. Bensimon, L. P. Kadanoff, S. Liang, B. I. Shraiman, and C. Tang, Rev. Mod. Phys. **58**, 977 (1986).

[5] P. G. Saffman, J. Fluid Mech. **173**, 73 (1986).

[6] G. M. Homsy, Ann. Rev. Fluid Mech. **19**, 271 (1987).

[7] J. S. Langer, Rev. Mod. Phys. **53**, 1 (1980).

[8] E. Ben-Jacob, R. Godbey, N. D. Goldenfeld, J. Koplik, H. Levine, T. Mueller, and L. M. Sander, Phys. Rev. Lett. **55**, 1315 (1985).

[9] Y. Couder, S. Michalland, M. Rabaud, and H. Thomé, in *Nonlinear Evolution of Spatio-Temporal Structures in Dissipative Continuous Systems*, edited by F. H. Busse and L. K. Kramer (Plenum, New York, 1990), p. 487.

[10] M. Rabaud, S. Michalland, and Y. Couder, Phys. Rev. Lett. **64**, 184 (1990).

[11] V. Hakim, M. Rabaud, H. Thomé, and Y. Couder, in *New Trends in Nonlinear Dynamics and Pattern Forming Phenomena: The Geometry of Nonequilibrium*, edited by P. Coullet and P. Huerre (Plenum, New York, 1990).

[12] Fisher Scientific Company, Fair Lawn, NJ.

[13] M. Rabaud, Y. Couder, and N. Gerard, Phys. Rev. A **37**, 935 (1988).

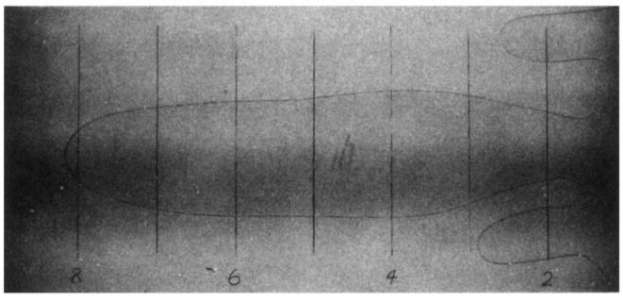

FIG. 1. Pattern formed in a Hele-Shaw cell with gap gradient $b' = -1.5 \times 10^{-3}$. If $b' = 0$, the finger would be stable at this driving velocity but would also be fatter at the tip and more uniform along its length.

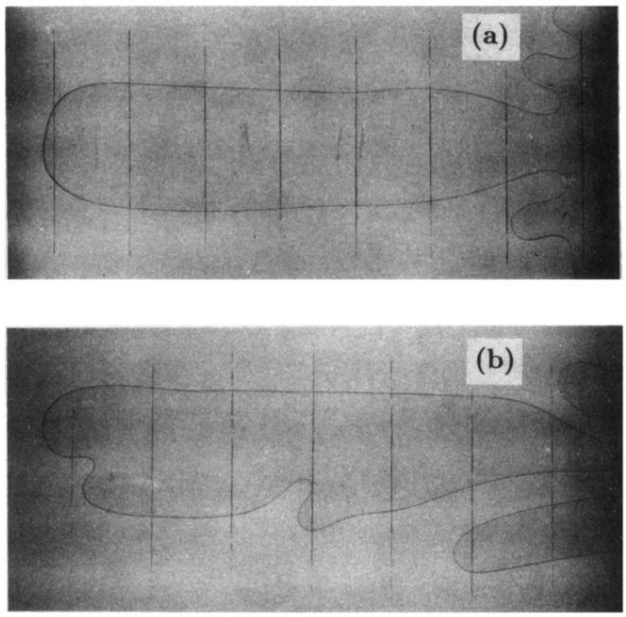

FIG. 2. Patterns formed in a Hele-Shaw cell with gap gradient $b' = 1.5 \times 10^{-3}$. (a) At low driving velocity, no tip-splitting occurs, but the finger exhibits a flattened tip. (b) Tip-splitting occurs at a driving velocity at which the finger would be stable if $b' = 0$.